Journal of Alloys and Compounds. Vol. 422. Núm. 1-2. 2006. Pag. 32-39
http://dx.doi.org/10.1016/j.jallcom.2005.12.004

Mössbauer study of a Fe-Zr-B-Cu-(Ge,Co) nanocrystalline alloy series

J. S. Blázquez, V. Franco, A. Conde

Dpto Fisica Materia Condensada, CSIC-Univ. Sevilla, Apt 1065, 41080 Sevilla, Spain

Keywords: Amorphous materials, nanostructured materials, Mössbauer spectroscopy.

Abstract. Amorphous and nanocrystalline Fe-Zr-B-Cu alloys with partial substitution of Co for Fe and Ge for B have been studied by Mössbauer spectrometry (MS). The compositional and microstructural dependence of the different hyperfine parameters were related to the results obtained by X-ray diffraction (XRD) and saturation magnetization measurements. Combination of MS and XRD leads to estimate an interface region, of thickness ~0.6 nm. The magnetic moment per transition metal of the crystalline phase is reduced with respect to binary crystalline alloys due to the existence of the interface.

*Corresponding author: Prof. A. Conde

Departamento de Física de la Materia Condensada. Universidad de Sevilla.

Apartado 1065, 41080 Sevilla (Spain).

Phone: (34) 95 455 28 85

Fax: (34) 95 461 20 97

E-mail: conde@us.es

Journal of Alloys and Compounds. Vol. 422. Núm. 1-2. 2006. Pag. 32-39
http://dx.doi.org/10.1016/j.jallcom.2005.12.004

1. Introduction

Very important attention has been devoted in the last two decades to the study of nanocrystalline Fe-based alloys due to their outstanding soft magnetic properties at room temperature [1]. The responsible for the ultrasoft magnetic properties (low coercivity of about ~1 A/m and high susceptibility of about ~10000) exhibited by these alloys is their characteristic two-phase microstructure. This microstructure consists of ferromagnetic nanocrystals of an α-Fe type phase (~10 nm in size) embedded in a residual amorphous phase, also ferromagnetic but with a lower Curie temperature. This specific configuration yields an averaging out of the magnetocrystalline anisotropy [2]. On the other hand, the magnetoelastic anisotropy can be minimized when the magnetostriction of the crystallites and that of the residual amorphous matrix are of different sign. The very small size of the crystallites provokes that an important amount of atoms are located at the boundary between the amorphous and the crystalline phases.

The typical composition of these alloys is Fe-M-ET-(Cu). M is a metalloid (generally B and, in some cases, Si), which facilitates the production of a precursor amorphous alloy and the nanocrystalline microstructure can be achieved after a controlled annealing process of this precursor alloy. ET is an early transition metal as Zr, Nb, Hf…, which impinges the growth of the crystals due to the combined effect of its very low solubility in the α-Fe phase and its slow diffusivity in the amorphous matrix. The presence of Cu is not always necessary to develop the nanocrystalline microstructure, especially in the alloys without Si, but it generally enhances the nucleation of the α-Fe phase refining the nanocrystalline microstructure by forming Cu-clusters at temperatures below the crystallization onset [3].

Concerning the composition, nanocrystalline Fe-based alloys can be divided into two families, with and without Si. In the former family, FINEMET-type, the presence of

Journal of Alloys and Compounds. Vol. 422. Núm. 1-2. 2006. Pag. 32-39
http://dx.doi.org/10.1016/j.jallcom.2005.12.004
Si inside the nanocrystals reduces the saturation magnetization and the Curie temperature of the crystalline phase. The family of alloys without Si, NANOPERM-type, yields a purer α-Fe phase than that of FINEMET.

Compositional tailoring of nanocrystalline alloys is still now a subject of intense study in order to improve their properties for specific applications. Particularly, the improvement of the performance for high temperature applications led to the development of HITPERM alloys in 1998 [4]. In these alloys, the partial substitution of Co for Fe strongly increases the Curie temperature of both crystalline and amorphous phases. However, the high magnetostriction of the crystalline α-FeCo phase impoverishes the soft magnetic character of the system at least in one order of magnitude [1,5]. Recently, Ge addition was proposed to improve the response of Fe-based nanocrystalline alloys at moderately high temperatures preserving the good specifications at room temperature [6]. Although Ge is soluble in the α-Fe phase up to 10 at. % [7], the benefits of its addition to the alloy are due to the preferential partition of this element to the residual amorphous phase.

The contribution of ^{57}Fe Mössbauer spectrometry to the study of Fe-based alloys has been very important as a local probe to determine the Fe environments, characterizing the microstructure and magnetic evolution of both crystalline and amorphous phases. In the case of NANOPERM systems, besides crystalline and amorphous phases, Mössbauer technique allows to distinguish a third contribution from the so-called interface region, associated to Fe atoms at the boundary of the nanocrystals which are affected by the atoms outside the crystal (Zr, B) [8]. The hyperfine fields ascribed to this contribution are higher than those expected for the amorphous region but can not be assigned to pure crystalline sites. The combination of Mössbauer

Journal of Alloys and Compounds. Vol. 422. Núm. 1-2. 2006. Pag. 32-39
http://dx.doi.org/10.1016/j.jallcom.2005.12.004
spectrometry with other experimental techniques allows a deeper knowledge of the parameters obtained.

In this work, the effect of Co and Ge addition on Fe-based alloys of the NANOPERM-type family has been studied using Mössbauer spectrometry, X-ray diffraction and saturation magnetization measurements. Results from the different techniques were combined to extract information about the three Mössbauer regions present in nanocrystalline alloys: amorphous, crystalline and interface.

2. Experimental

Amorphous ribbons (5 mm wide and 20-30 μm thick) of nominal composition $Fe_{83-X}Co_XZr_6B_{10-Y}Ge_YCu_1$ (X=0, 5, 20; Y=0, 5) were obtained by melt-spinning. For simplicity, the studied alloys will be named in the following only by their Co and Ge compositions (Co0Ge0, Co5Ge0, Co5Ge5 and Co20Ge5, respectively). Structurally-relaxed and nanocrystalline samples of the different studied alloys were obtained from as-cast samples after annealing in vacuum during 10 min at several temperatures (T_{ann}=698, 748, 798 and 873 K, respectively). Mössbauer (MS) spectra were recorded at room temperature in a transmission geometry using a ^{57}Co(Rh) source. The incident γ-beam was perpendicular to the ribbon plane. The values of the hyperfine parameters were obtained by fitting with NORMOS program [9]. The isomer shift, *I*, was quoted relative to the Mössbauer spectrum of an α-Fe foil at room temperature. The spectra of amorphous samples were fitted using a distribution of hyperfine fields, *H*. In the case of nanocrystalline samples, a set of discrete values of hyperfine fields and two hyperfine field distributions were used to fit the experimental data. The two hyperfine field distributions would roughly correspond to the amorphous phase and the interface region. The distinction between the limits of hyperfine fields corresponding to

amorphous and interface regions is ambiguous and thus overlapping between them was allowed in the fitting process. In the following, results will be given as the average between these two contributions as amorphous+interface contribution. In this work, MS spectra with crystalline sites contribution, A_C^{SITE}, below 10 % do not allow a precise study of the crystalline contribution (H, I, A_C^{SITE}); these spectra were fitted using only one distribution of H and one crystalline site. In all the studied cases, the quadrupolar splitting was negligible.

X-ray diffraction (XRD), using Co-Kα radiation, was performed on as-cast and annealed samples in order to determine their microstructure. Saturation magnetization, M_S, measurements were performed in a vibrating sample magnetometer (VSM) system applying a magnetic field of 0.5 T.

3. Results and discussion

3.1 Mössbauer spectrometry

Figures 1 shows the MS spectra of every as-cast and annealed samples of each studied alloy. The amorphous+interface and the crystalline contributions are shown along with the total fitting plot and the experimental data (circles). Figure 2 shows the thermal evolution of the probability of hyperfine fields, $P(H)$, for each studied alloy. Table 1 summarizes the results obtained after the fitting of the MS spectra.

3.1.1 Amorphous samples

The MS spectra of as-cast and annealed at 698 K samples show typical features of amorphous, as could be expected from the crystallization onset temperature of the studied alloys (in the range 737-783 K [10]). In such cases (squares and crosses plots in figure 2), the MS spectra were fitted using a single distribution of sextets. The main

difference between the as-cast and structurally relaxed amorphous samples is observed in the parameter R_{23}, which is the intensity ratio between the second and third lines of the sextets used to fit the spectrum. This parameter is related to the angle between the magnetic moments and the incident γ radiation, θ, as:

$$R_{23} = \frac{4\sin^2\theta}{1+\cos^2\theta} \quad (1)$$

After annealing at 698 K, structural relaxation occurs, yielding a decrease of the magnetic anisotropy due to the release of internal stresses. This is in agreement with the evolution of the magnetic moments orientation, turning out of plane, as can be seen in table 1. It is not possible to detect any dependence of R_{23} with the composition for the amorphous samples.

No difference can be detected between the $P(H)$ plots of as-cast and annealed at 698 K samples for the same composition. These plots can be described as two overlapped peaks (bimodal behaviour): one, almost independent of the composition, is centred around 10 T, whereas the other peak maximum shifts from 17 to 27 T as Co content increases in the alloy. This bimodal character and a similar compositional dependence were also observed for other Co containing amorphous Fe-based alloy series [11,12]. The high H region of the distributions must be due to Fe surrounded by Fe and Co atoms, preferentially. The low H values must be ascribed to Fe with some non magnetic atoms as nearest neighbour.

The $P(H)$ curve of the amorphous samples can be fitted using two Gaussian functions. It can be observed that the area of the first peak is about 10 % of the whole area for the alloys with 0 and 5 at. % of Co, but it decreases down to 5 % for Co20Ge5 alloy. The lower mixing enthalpy of Co with Zr than Fe with Zr (-41 and -25 kJ/mol, respectively) [13] would favour the preferential formation of Co-Zr environments with respect to the Fe-Zr environments. Therefore, although the concentration of Zr is

constant in the studied series, the probability of Fe atoms with Zr neighbours will decrease as Co content increases in the alloy and this effect becomes evident for 20 at. % of Co.

A clear increase of the average hyperfine field of the amorphous system, $<H>^{A}$, can be observed as the Co content increases in the alloy. However, the partial substitution of 5 at. % of Ge for B shows no effect on this parameter.

3.1.2 Nanocrystalline samples

For annealing temperatures equal or higher than 748 K, it is possible to observe the presence of high field contributions, which can be fitted using a discrete number of sextets and can be ascribed to the formation of the α-Fe type phase. The MS data indicate that the amount of this phase increases as the annealing temperature increases as can be expected and, for samples annealed during 10 min at 748 K, is significantly higher for Co20Ge5 and Co5Ge5 than for Co5Ge0 and Co0Ge0 alloys. This compositional effect can be explained from the values of the crystallization onset temperatures observed by differential scanning calorimetry (737, 758, 773 and 783 K, at 20 K/min, for Co20Ge5, Co5Ge5, Co5Ge0 and Co0Ge0, respectively [10]). In fact, the isothermal annealing reduces the onset temperature with respect to non-isothermal treatments. The XRD data that will be shown in the next section confirm the composition and thermal changes in crystalline fraction.

The MS spectra of nanocrystalline samples are more complex than those of the fully amorphous samples. In the cases in which the crystalline contribution is clearly observed (A_C^{SITE} >10 %), the average hyperfine field of the discrete sextets (crystalline sites contribution) is constant. Figure 3 shows the average values of *H* for the crystalline and the amorphous+interface contributions. In order to illustrate differences in the

thermal evolution of the amorphous and the interface, the average values of hyperfine fields below and above 20 T are also indicated.

For Co0Ge0 alloy, the average hyperfine field of crystalline sites contribution, $<H>^{C}$~33 T, is in agreement with that of the pure α-Fe phase. The value of the average isomer shift of the crystalline contribution for this alloy is also consistent with that of the pure α-Fe ($<I>^{C}$=0.00 mm/s). $<H>^{C}$ increases with the partial Co substitution for Fe up to ~34 T for 5 at. % of Co and up to ~35.5 T for 20 at. % of Co. The differences between Co5Ge0 and Co5Ge5 alloys are close to the error limit. From this point of view, the presence of Ge inside the nanocrystals can not be unambiguously established. The average value of the hyperfine field of the crystalline sites, $<H>^{C}$, for Co20Ge5 alloy is slightly smaller than that of α-$Fe_{80}Co_{20}$ (36 T [14]), which could be justified by the presence of a small amount of Ge inside the nanocrystals [15], as it was shown previously [10].

In the case of the amorphous+interface contribution to the *P(H)*, values in the range between 10 and 25 T progressively decrease as the annealing temperature increases, although the low and high fields contributions do not. This is also reflected in the thermal evolution of the average values of *H* below and above 20 T (see figure 3). Specifically, for Co0Ge0 alloy, new contributions, absent for amorphous samples, appear above 30 T, which can be ascribed to the formation of an interface region. This interface region would be formed by Fe atoms at the boundary of the nanocrystals. The hyperfine field of these atoms decreases with respect to that of the Fe atoms inside the nanocrystals by the presence of non magnetic atoms as nearest neighbours.

During the fitting, it is always possible to use more discrete sextets overlapping with the hyperfine distribution, which, in fact, is formed by a series of correlated discrete sextets. Therefore, it is convenient to assume some restrictions in the fitting in

order to avoid this ambiguity. The continuous distribution of hyperfine fields was limited to 32 T and the discrete sextets were fitted only with values of *H* higher than this limit. The goodness of this hypothesis will be tested in the following sections. In fact, Zr and B are rejected from the α-Fe lattice. Therefore, for Co0Ge0, the α-Fe phase must be fitted using only a sextet with *H*=33 T. The presence of Ge inside the nanocrystals must be reduced as far as this element preferentially partitions to the amorphous matrix [6,10] and the presence of Co increases the hyperfine field [14]. Therefore, *a priori*, this lower limit to the crystalline site contributions is not so strong. Other systems, such as FINEMET-type alloys (FeSiNbBCu composition), develop a crystalline α-Fe(Si) phase with lower *H* values of its crystalline sites, due to Si dissolved in the α-Fe phase. Therefore, the interface contribution could not be decoupled from low *H* crystalline sites, as can be done in the system object of this study [16].

The average isomer shift values of the crystalline contribution are close to that of pure α-Fe for the Co0Ge0, Co5Ge0 and Co5Ge5 alloys and slightly higher for the alloy with Co20Ge5. The observed values are consistent with the previously proposed compositions [10], considering the effect of Co [14] and Ge [15] in the α-Fe phase and the error bar of our experiments.

As it can be observed in table 1, the angle between the hyperfine field and the γ-radiation is larger for Co20Ge5 alloy than for the other three alloys. This nanocrystalline alloy shows higher coercivity (~40 A/m) than the other studied alloys (~10 A/m) [10], indicating a higher magnetic anisotropy.

3.2 Comparison with X-ray diffraction

Amorphous character of as-cast samples was checked by XRD. From MS results it could be found that nanocrystalline microstructure is developed in all the studied

alloys after annealing at 748 K (as an example, XRD patterns for Co5Ge5 alloy are shown in figure 4). However, XRD pattern could not detect the small amount of α-Fe formed in Co0Ge0 and Co5Ge0 alloy samples annealed at that temperature. Therefore, MS showed to be more sensitive than XRD in the detection of small crystalline fractions. This occurs in the studied alloy series because the external lines of the crystalline contribution in MS do not overlap with the amorphous contribution allowing a good resolution of the small crystalline peaks unlike for FINEMET-type alloys [16].

XRD patterns of all the studied alloys annealed at 798 and 873 K as well as of Co5Ge5 and Co20Ge5 alloy samples annealed at 748 K show the diffraction maxima of α-Fe phase along with an amorphous halo, typical of the two-phase (amorphous and crystalline) character of the nanocrystalline microstructure. No boride phase was detected in any of the studied samples. Table 2 summarizes the results extracted from XRD data. Crystalline volume fraction, X_C, was obtained after deconvoluting the amorphous halo and the (110) maximum of the α-Fe phase. The area ratio between the (110) diffraction maximum and the total intensity peak, X_C*, was corrected taking into account the average scattering powers of the two phases [17], estimated from the scattering factors of the different atoms at the angular position of the (110) maxima and the Co Kα wavelength (~2 for B, ~20 for Fe, Co, Ge or Cu and ~30 for Zr [18]). Knowing that Zr and B are rejected from the crystalline phase, the correction factor, $F=X_C/X_C$*, is 0.9 for the alloys without Ge and 1 for the alloys with Ge. The grain size, D, was estimated using Scherrer formula and the lattice parameter, a, was calculated from the angular position of the (110) and (200) diffraction maxima.

From figure 5, it is possible to observe a linear correlation between A_C^{SITE} (the fraction of Fe atoms in crystalline sites of the total number of Fe atoms in the material, derived from MS) and X_C (the crystalline volume fraction, derived from XRD) for each

alloy. These two magnitudes can be linked. If the difference in density of the amorphous and nanocrystalline samples is neglected, X_C can be written as:

$$X_C = \frac{N_C < V_{at}^C >}{N_T < V_{at}^T >} \tag{2}$$

where N_C is the number of atoms in the crystalline phase and N_T is the total number of atoms, $< V_{at}^C >$ is the average atomic volume of the crystalline phase and $< V_{at}^T >$ is the average atomic volume of the whole material.

On the other hand:

$$A_C = A_C^{SITE} + A_C^{INT} = \frac{N_C^{Fe}}{N_T^{Fe}} = \frac{N_C C_C^{Fe}}{N_T C_T^{Fe}} \tag{3}$$

where A_C is the fraction of Fe atoms in the crystalline phase, considering the contribution of the atoms at the interface, A_C^{INT}, which, in fact, do contribute to the X-ray diffraction, as these atoms are located in the crystalline lattice; N_C^{Fe} is the number of Fe atoms in the crystalline phase, N_T^{Fe} is the total number of Fe atoms, C_C^{Fe} is the concentration of Fe in the crystalline phase and C_T^{Fe} is the average concentration of Fe in the alloy. Therefore:

$$A_C = X_C \frac{C_C^{Fe} < V_{at}^T >}{C_T^{Fe} < V_{at}^C >} = X_C \frac{C_C^{Fe}}{C_T^{Fe}} \left(\frac{< r_{at}^T >}{< r_{at}^C >} \right)^3 \tag{4}$$

Being $< r_{at}^T >$ and $< r_{at}^C >$ the average atomic radii of the whole alloy and of the crystalline phase, respectively.

The interface is a thin layer at the boundary of the nanocrystal, where the hyperfine field of Fe atoms in bcc lattice is affected by the vicinity of Zr and B atoms. Assuming spherical nanocrystals with a diameter *D* and an interface thickness *t*, it is possible to write:

$$A_C = A_C^{SITE} \frac{D}{D-6t} \tag{5}$$

from which:

$$A_C^{SITE} = X_C \frac{C_C^{Fe}}{C_T^{Fe}} \left(\frac{< r_{at}^T >}{< r_{at}^C >} \right)^3 \frac{(D-6t)}{D} \tag{6}$$

A_C^{SITE} was obtained after fitting the MS (see table 1), X_C and D were obtained from XRD (see table 2), the atomic radii used were the Goldschmidt values [19], C_T^{Fe} is the nominal Fe composition of the alloy and C_C^{Fe} can be estimated from previous results [10]. Therefore, from the above expression it can be estimated the thickness of the interface, *t*. Table 3 summarizes the results obtained from (6). For Ge containing alloys, two limit cases were considered: 0 % Ge and 5 % Ge inside the nanocrystals. The value of *t* does not significantly change between these two cases.

For Co0Ge0, Co5Ge0 and Co20Ge5 alloys, the value of *t* is approximately 0.6 nm, which roughly correspond to 2-3 atomic layers. This result is physically meaningful as far as the Zr atoms are expected to pile up at the nanocrystals boundary and it is not surprising that this high concentration of Zr affects the Fe atoms in a layer of 0.6 nm (practically only nearest neighbour and next nearest neighbour shells would affect *H*). However, the Co5Ge5 alloy shows a higher value of *t*. This could be due to an underestimation of the crystalline sites contribution which was restricted to values of *H* >32 T. If some Ge atoms were dissolved into the α-Fe phase, and considering the low content of Co, it is possible to have crystalline sites with *H*<33 T [15] and which were fitted by the continuous distribution of hyperfine fields. In the case of Co20Ge5 alloy, the high content of Co yields to higher *H* values for the crystalline sites of Fe atoms.

3.3 Comparison with saturation magnetization measurements

Journal of Alloys and Compounds. Vol. 422. Núm. 1-2. 2006. Pag. 32-39
http://dx.doi.org/10.1016/j.jallcom.2005.12.004

Saturation magnetization, M_S, was measured in a VSM system under an applied magnetic field of 0.5 T. From these values, the average magnetic moment per transition metal, $<\mu_{TM}>$, can be calculated. Figure 6 shows the average value of hyperfine field as a function of $<\mu_{TM}>$. A clear linear correlation can be observed between these two magnitudes for all the studied samples.

Although similar linear correlations have been reported for amorphous and crystalline alloys [11,20], it is worth noticing that, in this study, the linear correlation between $<H>$ and $<\mu_{TM}>$ is observed for systems with different amount of crystalline and amorphous phases, characterized by the value of X_C. Figure 7 clarifies this point. This figure shows that both magnitudes $<H>$ and $<\mu_{TM}>$ show very similar evolution with the crystalline volume fraction, which might cancel the dependency on this parameter in the plot of figure 6.

From figure 7, a linear relationship between $<\mu_{TM}>$ and X_C can be approximated for each composition. The average magnetic moment per atom, $<\mu>$, takes into account those which are not transition metal atoms and can be divided in two contributions: amorphous and crystalline phase as:

$$<\mu>= X_C <\mu>^C +(1-X_C)<\mu>^A \quad (7)$$

where $<\mu>^C$ and $<\mu>^A$ are the average magnetic moment per atom in the nanocrystals and in the amorphous matrix, respectively. The composition of the crystalline phase can be considered constant along the nanocrystallization and, in Ge free alloys, $<\mu>^C=<\mu_{TM}>^C$, where $<\mu_{TM}>^C$ is the magnetic moment per transition metal atom (Fe and Co) in the crystalline phase. However, as nanocrystallization progresses, the concentration of Fe, and thus of transition metal, is reduced in the amorphous matrix so $<\mu>^A$ can not be considered constant as X_C increases. Nevertheless, this magnitude can

be expressed as a function of the magnetic moment per transition metal in the amorphous matrix, $<\mu_{TM}>^{A}$ as:

$$<\mu>^{A} = C_{TM}^{A} <\mu_{TM}>^{A} = \frac{C_{TM}^{T} - C_{TM}^{C} X_C}{1 - X_C} <\mu_{TM}>^{A} \quad (8)$$

where C_{TM}^{A}, C_{TM}^{C} and C_{TM}^{T} are the concentration of transition metal in the amorphous matrix, the nanocrystals and the whole system, respectively.

Taking into account that $<\mu>= C_{TM}^{T} <\mu_{TM}>$ and combining equations (7) and (8), it is possible to write:

$$<\mu_{TM}>= \frac{1}{C_{TM}^{T}} \left(<\mu_{TM}>^{C} - <\mu_{TM}>^{A}\right) X_C + <\mu_{TM}>^{A} \quad (9)$$

where the Ge content inside the nanocrystals has been neglected, resulting in $C_{TM}{}^{C}$=1, which is only an approximation for Ge-containing alloys. However, as in this study no difference can be observed between Co5Ge0 and Co5Ge5 alloys, the effect of this approximation seems to be smaller than the error bar.

Figure 8 shows the values of the different magnetic moments estimated from expression (9) as a function of the Co content of the alloy. The magnetic moments per atom in binary bcc FeCo alloys [21] are also indicated for comparison. It is worth noticing that the average values of the magnetic moment in the nanocrystals are below those of the corresponding bcc phase in binary alloys. This can be explained by the presence of the interface region detected by Mössbauer technique. In fact, although the atoms in this region are in the crystalline lattice, their magnetic moments must be reduced by the neighbouring of Zr and B atoms located in the amorphous matrix.

4. Conclusions

Journal of Alloys and Compounds. Vol. 422. Núm. 1-2. 2006. Pag. 32-39
http://dx.doi.org/10.1016/j.jallcom.2005.12.004

Mössbauer spectrometry was used in combination with X-ray diffraction and saturation magnetization measurements in order to explore the effect of partial substitution of Co for Fe and Ge for B in a Fe-Zr-B-Cu alloy series.

The nanometer size of the crystallites provokes the formation of three regions observed by Mössbauer spectrometry: amorphous matrix, interface and crystalline region. In this study, interface region has been considered formed only by those Fe atoms in the crystalline lattice which magnetically feel the presence of non-magnetic atoms outside the nanocrystals.

Combination of MS and XRD technique yields an estimation of the interface thickness as 0.6 nm (2-3 atomic layers).

Combination of MS, XRD and saturation magnetization measurements yields an estimation of the evolution of the magnetic moments in the amorphous and crystalline phases.

Acknowledgments

This work was partially supported by the Spanish Government and EU FEDER (Project MAT 2004-04618) and by the PAI of the Reginal Government of Andalucía (Spain). J.S.B. acknowledges a research contract from this Regional Government.

Journal of Alloys and Compounds. Vol. 422. Núm. 1-2. 2006. Pag. 32-39
http://dx.doi.org/10.1016/j.jallcom.2005.12.004

References

[1] M. E. McHenry, M. A. Willard, D. E. Laughlin, Prog. Mater. Sci. 44 (1999) 291.

[2] G. Herzer, IEEE Trans. Magn. 25 (1989) 3327.

[3] K. Hono, Prog. Mater. Sci. 47 (2002) 621.

[4] M. A. Willard, D. E. Laughlin, M. E. McHenry, D. Thoma, K. Sickafus, J. O. Cross, V. G. Harris, J. Appl. Phys. 84 (1998) 6773.

[5] J. S. Blázquez, V. Franco, A. Conde, M. R. J. Gibbs, H. A. Davies, Z. C. Wang, J. Magn. Magn. Mat. 250 (2002) 260.

[6] K. Suzuki, J. W. Cochrane, J. M. Cadogan, X. Y. Xiong, K. Hono, J. Appl. Phys. 91 (2002) 8417.

[7] Massalski TB, Okamoto H, Subramanian PR, Kacprzak L. Binary Alloys Phase Diagrams. Materials Park, Ohio: ASM International, 1992.

[8] M. Miglierini, J. M. Grenèche, J. Phys.: Cond. Matter, 9 (1997) 2321.

[9] R. A. Brand, J. Lauer, D. M. Herlach, J. Phys. F: Met. Phys. 12 (1983) 675.

[10] J. S. Blázquez, S. Roth, C. Mickel, A. Conde, Acta Mater. 53 (2005) 1241.

[11] J. M. Borrego, C. F. Conde, A. Conde, S. Roth, J. Eckert, J. M. Grenèche, J. Appl. Phys. 95 (2004) 4151.

[12] J. S. Blázquez, J. M. Borrego, C. F. Conde, A. Conde, J. M. Grenèche, J. Phys.: Cond. Matter 15 (2003) 3957.

[13] F. R. de Boer, R. Boom, W. C. M. Mattens, A. R. Miedema, A. K. Niessen. Cohesion in Metals. Transition Metals Alloys. Amsterdam: North-Holland; 1989.

[14] H. H. Hamdeh, J. Okamoto, B. Fultz, Phys. Rev. B 42 (1990) 6694.

[15] G. N. Konygin, E. P. Yelsukov, V. E. Porsev, J. Magn. Magn. Mat. 288 (2005) 27.

[16] J. M. Grenèche, M. Miglierini, A. Slawska-Waniewska, Hyperfine Interact. 126 (2000) 27.

[17] J. S. Blázquez, V. Franco, C. F. Conde, A. Conde, J. Magn. Magn. Mat. 254-255 (2003) 460.

[18] B. D. Cullity. Elements of X-ray Diffraction. Reading: Addison-Wesley, 1956. p. 474.

[19] C. J. Smithells. Metals Reference Book, vol. 1. London: Butterworths, 1967. p. 100.

[20] S. Dey, P. Deppe, M. Rosenberg, F. E. Luborsky, J. L. Walter, J. Appl. Phys. 52 (1981) 1805.

[21] H. H. Hamdeh, B. Fultz, D. H. Pearson, Phys. Rev. B 39 (1989) 11233.

Journal of Alloys and Compounds. Vol. 422. Núm. 1-2. 2006. Pag. 32-39
http://dx.doi.org/10.1016/j.jallcom.2005.12.004

Table 1. Mössbauer parameters.

Comp.	T_{ann}	$<H>^A$	$<H>^C$	$<I>^A$	$<I>^C$	A_C^{SITE}	R_{23}	θ
	(K)	±0.2 T		±0.01 mm/s		±5%	±0.2	(º)
Co0Ge0	300	15.7	-	-0.03	-	-	2.5	61
	698	15.4	-	-0.04	-	-	2.0	55
	748	16.2	32.3	-0.04	0.03	0.02	1.3	44
	798	19.1	33.1	-0.01	0.01	0.31	1.2	43
	873	18.8	33.1	0.00	0.01	0.40	1.2	43
Co5Ge0	300	20.3	-	-0.01	-	-	2.4	60
	698	20.5	-	0.02	-	-	1.3	44
	748	20.6	33.9	0.02	0.06	0.07	1.7	51
	798	19.6	34.1	0.01	0.01	0.38	0.9	37
	873	18.9	34.0	0.01	0.02	0.46	1.3	44
Co5Ge5	300	20.9	-	0.00	-	-	2.6	63
	698	20.4	-	0.01	-	-	1.9	53
	748	20.9	33.6	0.03	0.02	0.23	2.4	60
	798	21.6	33.9	0.05	0.03	0.39	1.0	39
	873	21.0	33.9	0.03	0.02	0.44	1.9	53
Co20Ge5	300	26.4	-	0.03	-	-	2.5	61
	698	27.1	-	0.04	-	-	1.8	52
	748	21.8	35.5	0.06	0.04	0.49	2.8	65
	798	20.9	35.5	0.04	0.03	0.57	2.9	66
	873	21.1	35.6	0.06	0.04	0.62	2.6	63

Journal of Alloys and Compounds. Vol. 422. Núm. 1-2. 2006. Pag. 32-39
http://dx.doi.org/10.1016/j.jallcom.2005.12.004

Table 2. X-ray diffraction results.

Composition	T_{ann} (K)	X_C (± 0.05)	D (± 2 nm)	a (± 0.0005 nm)
Co0Ge0	798	0.56	7	0.2868
	873	0.74	8	0.2865
Co5Ge0	798	0.61	7	0.2866
	873	0.75	8	0.2865
Co5Ge5	748	0.45	7	0.2876
	798	0.72	9	0.2876
	873	0.83	9	0.2876
Co20Ge5	748	0.66	8	0.2878
	798	0.77	9	0.2875
	873	0.82	9	0.2870

Journal of Alloys and Compounds. Vol. 422. Núm. 1-2. 2006. Pag. 32-39
http://dx.doi.org/10.1016/j.jallcom.2005.12.004

Table 3. Estimation of the interface thickness from expression (6).

Composition	$\frac{A_C^{SITE}}{X_C}$	$\frac{C_T^{Fe}}{C_C^{Fe}}$	$\left(\frac{< r_{at}^T >}{< r_{at}^C >}\right)^3$	<D> (nm)	t (nm)
Co0Ge0	0.53	100/83	0.97	7.3	0.66
Co5Ge0	0.62	95/78	0.97	7.3	0.58
Co5Ge5	0.53	95/78*	1.02	8.3	0.80
		90/78**	1.01		0.76
Co20Ge5	0.76	80/63*	1.02	8.5	0.59
		75/63**	1.01		0.52

* Assuming 0 at. % of Ge inside the nanocrystals.

** Assuming 5 at. % of Ge inside the nanocrystals.

Journal of Alloys and Compounds. Vol. 422. Núm. 1-2. 2006. Pag. 32-39
http://dx.doi.org/10.1016/j.jallcom.2005.12.004

Figure captions

Figure 1. Experimental and fitted MS spectra of as-cast and annealed samples of the different studied alloys. Amorphous+interface and crystalline sites contributions are also shown.

Figure 2. Hyperfine field probability distribution for the different studied samples. Plots for each alloy are divided in two contributions: amorphous+interface (distribution) and crystalline sites (discrete values). Note that the Y-axis scales are different.

Figure 3. Average hyperfine field values for amorphous+interface (squares) and crystalline (down triangle) contributions. In Amorphous+interface contribution has been divided in averaging over values higher than 20 T (up triangle) and lower than 20 T (circles).

Figure 4. XRD patterns of Co5Ge5 samples annealed at different temperatures.

Figure 5. Fraction of Fe atoms in crystalline sites versus crystalline volume fraction.

Figure 6. Average hyperfine field versus average magnetic moment per transition metal atom.

Figure 7. Average hyperfine field and average magnetic moment per transition metal atom versus crystalline volume fraction.

Figure 8. Average magnetic moment per transition metal atom for amorphous (squares) and crystalline (circles) phases versus the Co content of the alloy. The values of binary α-FeCo phase are also indicated for comparison.

Journal of Alloys and Compounds. Vol. 422. Núm. 1-2. 2006. Pag. 32-39
http://dx.doi.org/10.1016/j.jallcom.2005.12.004

Figure 1

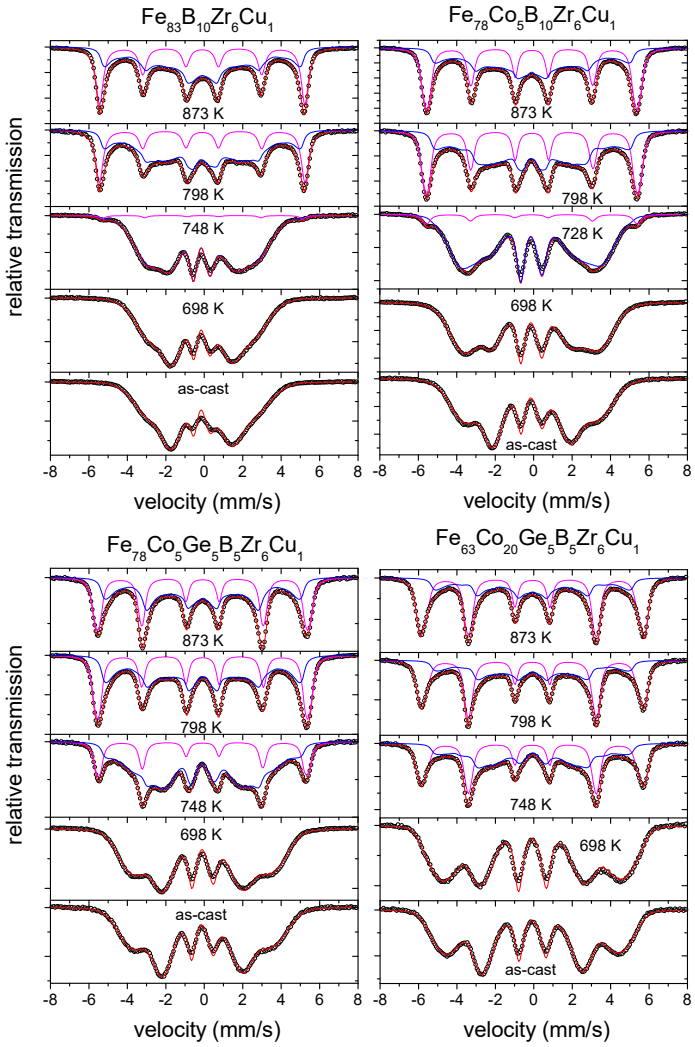

Journal of Alloys and Compounds. Vol. 422. Núm. 1-2. 2006. Pag. 32-39
http://dx.doi.org/10.1016/j.jallcom.2005.12.004

Figure 2

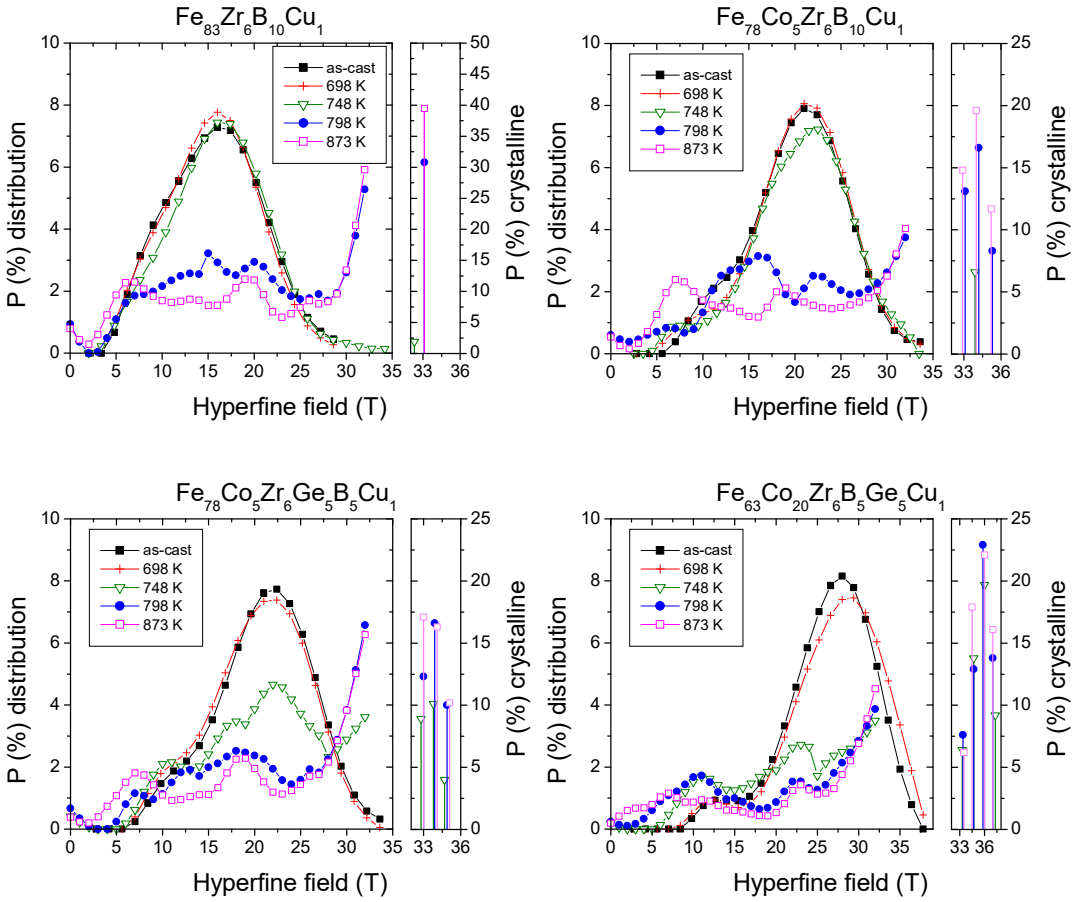

Journal of Alloys and Compounds. Vol. 422. Núm. 1-2. 2006. Pag. 32-39
http://dx.doi.org/10.1016/j.jallcom.2005.12.004

Figure 3

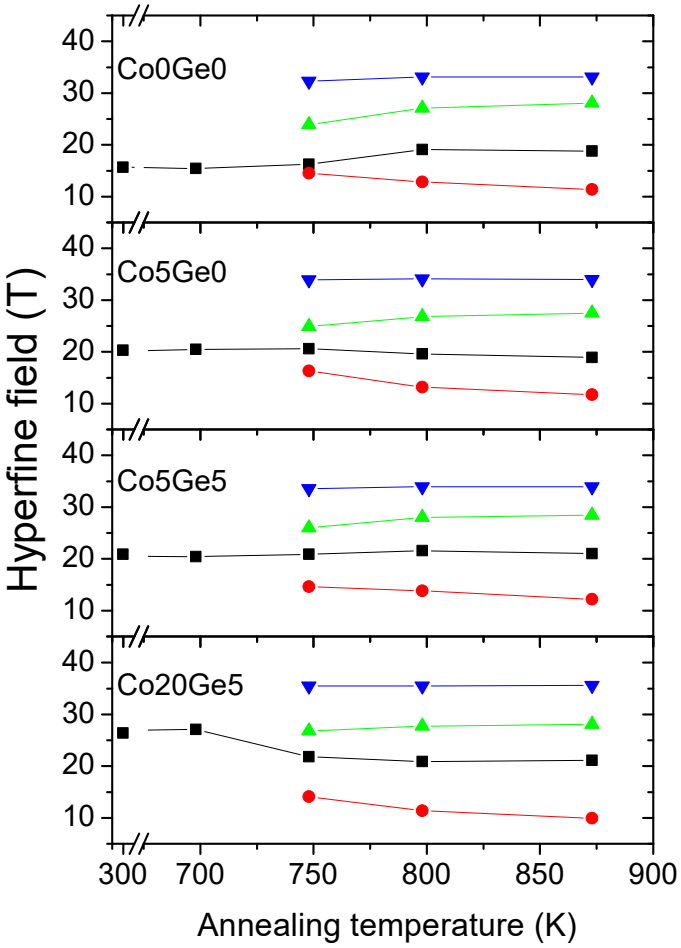

Journal of Alloys and Compounds. Vol. 422. Núm. 1-2. 2006. Pag. 32-39
http://dx.doi.org/10.1016/j.jallcom.2005.12.004

Figure 4

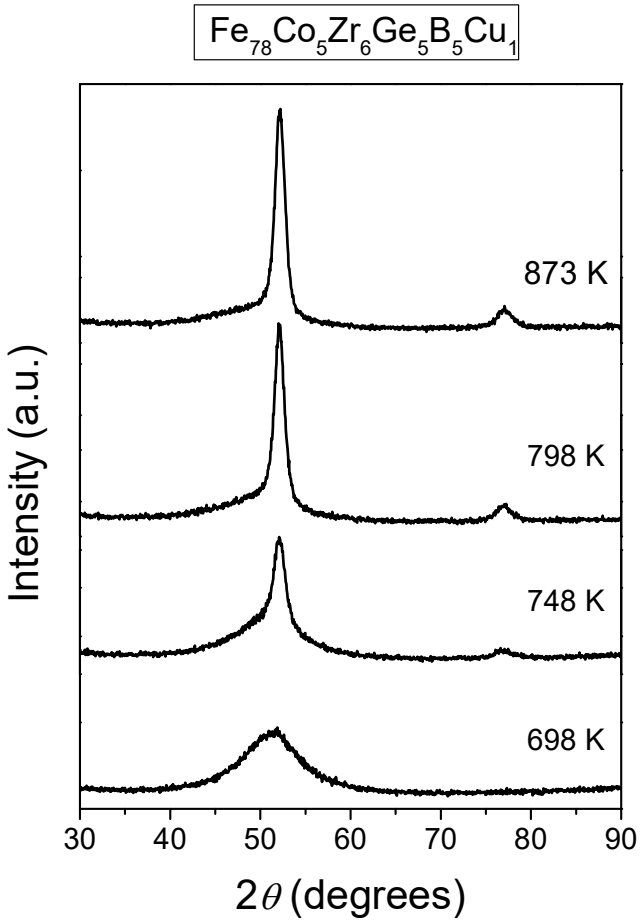

Journal of Alloys and Compounds. Vol. 422. Núm. 1-2. 2006. Pag. 32-39
http://dx.doi.org/10.1016/j.jallcom.2005.12.004

Figure 5

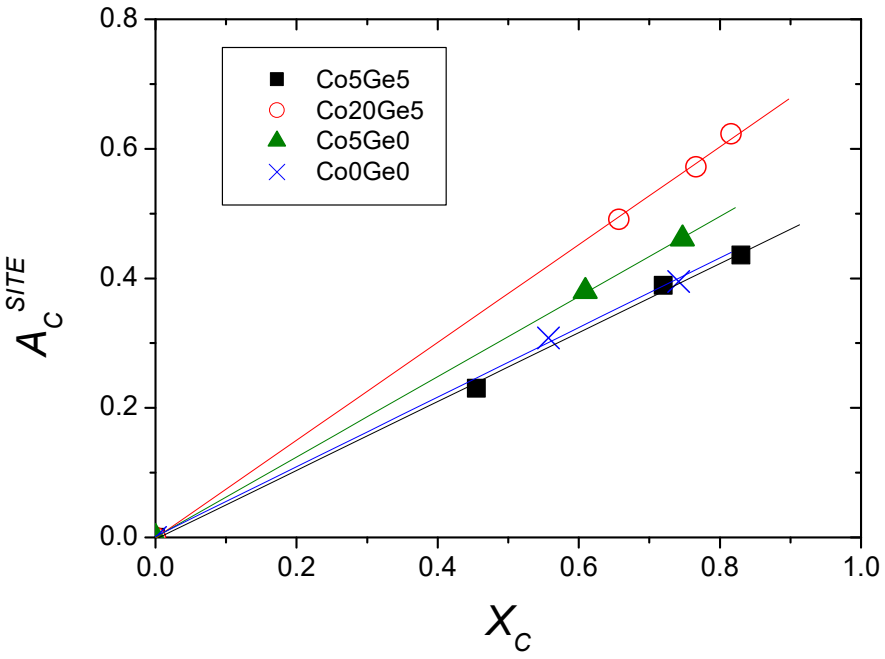

Journal of Alloys and Compounds. Vol. 422. Núm. 1-2. 2006. Pag. 32-39
http://dx.doi.org/10.1016/j.jallcom.2005.12.004

Figure 6

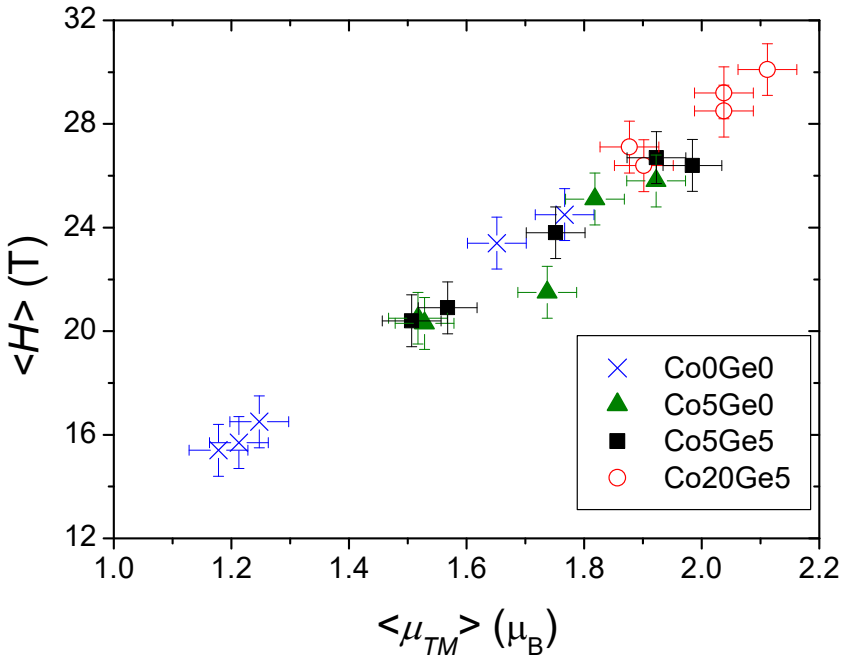

Journal of Alloys and Compounds. Vol. 422. Núm. 1-2. 2006. Pag. 32-39
http://dx.doi.org/10.1016/j.jallcom.2005.12.004

Figure 7

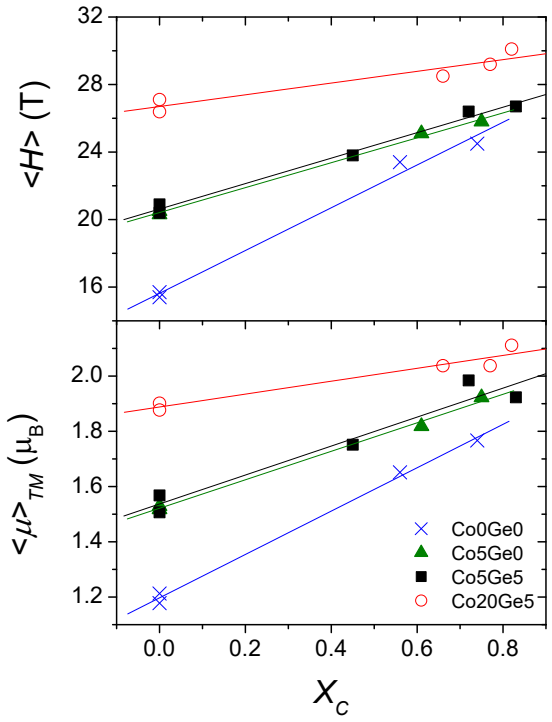

Journal of Alloys and Compounds. Vol. 422. Núm. 1-2. 2006. Pag. 32-39
http://dx.doi.org/10.1016/j.jallcom.2005.12.004

Figure 8